

Molecular Dosimetry of Temozolomide: Quantification of Critical Lesions, Correlation to Cell Death Responses, and Threshold Doses



Björn Stratenwerth¹, Susanne M. Geisen², Yang He¹, Lea Beltzig¹, Shana J. Sturla², and Bernd Kaina¹

ABSTRACT

Temozolomide (TMZ) is a DNA-methylating agent used in cancer chemotherapy, notably for glioblastoma multiforme (GBM), where it is applied as a front-line drug. One of the DNA alkylation products of TMZ is the minor lesion *O*⁶-methylguanine (*O*⁶MeG), which is responsible for nearly all genotoxic, cytotoxic, and cytostatic effects induced in the low-dose range relevant for cancer therapy. Here, we addressed the question of how many *O*⁶MeG adducts are required to elicit cytotoxic responses. Adduct quantification revealed that *O*⁶MeG increases linearly with dose. The same was observed for DNA double-strand breaks (DSB) and p53ser15. Regarding apoptosis, hockeystick modeling indicated a possible threshold for A172 cells at 2.5 μmol/L TMZ, whereas for LN229 cells no threshold was detected. Cellular senescence, which is the main

cellular response, also increased linearly, without a threshold. Using a dose of 20 μmol/L, which is achievable in a therapeutic setting, we determined that 14,000 adducts give rise to 32 DSBs (γH2AX foci) in A172 cells. This leads to 12% cell death and 35% of cells entering senescence. In LN229 cells, 20 μmol/L TMZ induced 20,600 *O*⁶MeG adducts, 66 DSBs (γH2AX foci), 24% apoptosis, and 52% senescence. The linear dose response and the genotoxic and cytotoxic effects observed at therapeutically relevant dose levels make it very likely that the TMZ target concentration triggers a significant cytotoxic and cytostatic effect *in vivo*. Despite a linear increase in the *O*⁶MeG adduct level, DSBs, and p53 activation, the low curative effect of TMZ results presumably from the low rate of apoptosis compared to senescence.

Introduction

Temozolomide (TMZ) is a DNA-methylating agent frequently used in cancer therapy (1). It is applied in first-line therapy for high-grade gliomas, including astrocytoma (WHO grade 3) and glioblastoma multiforme (GBM; glioma WHO grade 4; ref. 2) and in some other cancers (3). TMZ is a triazene derivative that does not need metabolic activation. It decomposes spontaneously yielding 3-methyl-(triazene-1-yl)imidazole-4-carboxamide (MTIC) and, in a second step, 5-aminoimidazole-4-carboxamide (AIC) and monomethyl hydrazine, which finally methylates DNA at various sites. As revealed by studies with DNA repair mutants and isogenic cell lines (4, 5), the main genotoxic and cytotoxic target of TMZ is the nuclear DNA. Similar to other S_N1 alkylating agents, at least 12 nucleophilic sites are subject of methylation (6). The major methylation products are *N*-methylpurines such as *N*7-methylguanine, *N*3-methylguanine, and *N*3-methyladenine (comprising about 80% of total alkylation), whereas *O*-methylpurines are less frequent. Thus, *O*⁶-methylguanine (*O*⁶MeG) accounts for only 7% of the total DNA methylation (6). Although produced in minor amounts, *O*⁶MeG is the main mutagenic, carci-

nogenic, genotoxic, and cytotoxic lesion (reviewed in ref. 7). It is also responsible for autophagy and cellular senescence, which are endpoints induced by TMZ concomitant to apoptosis (8).

*O*⁶MeG is repaired by the suicide enzyme *O*⁶-methylguanine-DNA methyltransferase (MGMT) in a damage reversal reaction (9). If cells are repair competent, *O*⁶MeG is quickly removed from DNA whereas in repair-incompetent cells, *O*⁶MeG persists. Because *O*⁶MeG is not eliminated by spontaneous hydrolysis, it can be transmitted even to the next cell generation, exerting long-term effects (10). The MGMT gene is a subject of intensive genetic and epigenetic regulation and therefore cells and tissues vary considerably in their repair capacity (11–13). High expression levels were observed in liver and the lowest in brain (13). Brain tissue of rats is completely devoid of MGMT, leading to persistence of *O*⁶MeG, which is the reason for neurotropic carcinogenesis following exposure with S_N1 methylating agents such as *N*-methyl-*N*-nitrosourea (14). The human brain expresses MGMT, although at low levels compared with other organs (15, 16). About 40% of human brain cancer (glioma grade 3 and 4) show MGMT promoter hypermethylation, which is related to MGMT downregulation, and 17% of GBM are completely devoid of MGMT repair activity as determined in an enzymatic assay (17). Therefore, promoter-methylated GBM are responsive to TMZ therapy (18–20).

In MGMT repair-competent cells, higher doses of TMZ are required to be cytotoxic, which results from non-repaired *N*-alkylation lesions that interfere with the replication machinery (21). These lesions are repaired by base excision repair (BER) and ALKB homologous proteins (ALKBH; ref. 7) and, therefore, they do not contribute to cytotoxicity if *O*⁶MeG is left in the DNA. However, if at high TMZ dose levels the *N*-alkylation repair system is saturated, these lesions contribute to cell death as well. The doses of TMZ in a therapeutic setting are very likely too low to achieve cell death resulting from *N*-alkylation products. Therefore, with a serum concentration of ~50 μmol/L TMZ, the *O*⁶MeG adducts are the key players inducing tumor cell death.

¹Institute of Toxicology, University Medical Center, University Mainz, Mainz, Germany. ²Department of Health Sciences and Technology, ETH Zürich, Zürich, Switzerland.

Note: Supplementary data for this article are available at Molecular Cancer Therapeutics Online (<http://mct.aacrjournals.org/>).

Corresponding Author: Bernd Kaina, Institute of Toxicology, Medical Center of the University Mainz, Obere Zahlbacher Str. 67, Mainz D-55131, Germany. E-mail: kaina@uni-mainz.de

Mol Cancer Ther 2021;20:1789–99

doi: 10.1158/1535-7163.MCT-21-0228

This open access article is distributed under Creative Commons Attribution-NonCommercial-NoDerivatives License 4.0 International (CC BY-NC-ND).

©2021 The Authors; Published by the American Association for Cancer Research

The mechanisms of O^6 MeG triggered cell death responses have been investigated intensively (22). In brief, a widely accepted model claims that O^6 MeG is a mutagenic mispairing lesion resulting in mismatches with thymine that are subject to mismatch repair (MMR). Reinsertion of thymine during MMR causes a futile MMR cycle, resulting in gaps in the DNA that finally give rise to DNA replication blockage and the formation of replication-mediated DNA double-strand breaks (DSB). This occurs in the posttreatment cell cycle, which is compatible with the time-course of apoptosis and DSB formation (23). Results obtained with synchronized cells confirmed this model (10). It is further known that DSBs induced by the processing of O^6 MeG/thymine trigger complex DNA damage response pathways, which are activated primarily by ATR, and secondary by ATM, and downstream CHK1 and CHK2, respectively (24) as well as activation of the SIAH1-HIPK2-p53 axis (25). In this scenario, the following factors determine drug resistance: MGMT, MMR, the proliferation level, DNA damage response (DDR) activation, and DSB repair by homologous recombination. O^6 MeG is not only an apoptosis-inducing damage, it also triggers with high efficiency cellular senescence in glioblastoma cells (8). The pathways involved were described previously (8, 26, 27).

Patients suffering from GBM, which make up ~70% of high-grade malignant gliomas, have a dismal prognosis (2). Standard therapy includes resection of the tumor followed by radiotherapy and concomitant chemotherapy with TMZ (28). TMZ is also prescribed in the recurrent situation and as maintenance therapy, and is well tolerated even if treatment occurs daily over long periods of time (29). In view of the bad prognosis and weak therapeutic efficiency of TMZ, better knowledge of the action of this anticancer drug is highly desirable. Given the known mechanism of action of TMZ, some questions arise which are a matter of debate (27, 30). First, do GBM cells die (by apoptosis or other forms of cell death) following TMZ treatment or does the drug exert only a cytostatic effect? Second, are the doses used for patient's treatment high enough to kill cancer cells without having toxic side effects on non-cancer cells? This question relates to the paradigm that low doses of a genotoxic anticancer drug are ineffective and that presumably thresholds exist below which cytotoxicity does not occur. Finally, third, how many O^6 MeG adducts are required for eliciting a specific effect such as apoptosis, necrosis, and senescence and can this level be achieved *in vivo*?

To address these fundamental questions in the molecular dosimetry of TMZ, we measured the amount of O^6 MeG induced by TMZ in established GBM cell lines and related this to levels of DSBs, apoptosis, necrosis, overall cell death, and cellular senescence. The data revealed that the amount of O^6 MeG following TMZ exposure, similar to DSBs, increased linearly with dose. Likewise, cell death, and senescence tracked with the formation of these damage products. Finally, we found that even at low-dose levels genotoxic, cytotoxic, and cytostatic effects were induced by TMZ. The amount of lesions inducing a particular effect was determined.

Materials and Methods

Cell lines and culture conditions

The human glioblastoma cell lines LN229 and A172 were purchased from ATCC, expanded, stored frozen in batches, and kept in culture only for limited time periods (maximally 2 month). LN229-MGMT (clone 12) was generated by stable transfection of LN229 with a human MGMT cDNA expression vector as described previously (8, 31). Cells were cultured in DMEM with Glutamax (Gibco, Life Technologies Corporation) and 10% fetal calf serum at 37°C in a humidified 5% CO₂ atmosphere and routinely checked for mycoplasma contamination

using a Kit (Venor GeM Classic) from Minerva Biolabs. Cells were seeded 48 hours before treatment, when they reached exponential growth. For short-term experiments (harvest 3 days after treatment), 2×10^5 cells were seeded per 5-cm or 6-well dish (in 5 or 4 mL medium, respectively), for long-term experiments (apoptosis and senescence following TMZ) 1×10^5 cells were seeded per dish. Under these conditions, cells were kept in exponential growth for the whole experimental period.

Drugs and drug treatment

TMZ obtained from Dr. Geoff Margison (University of Manchester) was dissolved in DMSO (150 mmol/L stock) and stored in batches at -80°C until use. Immediately before use, it was diluted 1:10 in sterile distilled water and added to the cell culture medium at the desired final concentration. For low final concentrations ($\leq 10 \mu\text{mol/L}$), the solution was further diluted with distilled water to a 1 mmol/L stock solution. Water-diluted stocks were used only once. The amount of DMSO in the medium did not exceed 0.05% and was without any cytotoxic effect (controls).

Quantification of O^6 MeG adducts

O^6 MeG adduct quantification was performed by measuring O^6 -methyl-deoxyguanosine (O^6 MeG), which was normalized to the deoxyguanosine (dG) content (32), according to a modified method as recently described in detail (33). Briefly, exponentially growing cells were treated with TMZ and cells were harvested at the time points indicated by trypsinization. Cells were taken up in complete medium, washed with PBS before the cell pellet was stored frozen at -80°C. DNA from cell pellets with a defined cell number was isolated using the QIAamp DNA Mini Kit (Qiagen). Briefly, lysis buffer, proteinase K, and RNase A were added and cell pellets were incubated for 20 minutes at 56°C, 1,400 rpm on a ThermoShaker. Afterwards, ethanol was added and DNA was purified and extracted on spin columns applying washing buffers and MilliQ for elution according to the manufacturer's instruction. Internal labelled standards were added to the sample and DNA was enzymatically hydrolyzed, yielding free nucleosides. Following further sample clean-up by solid-phase extraction, O^6 MeG was quantified by reversed-phase nano-liquid chromatography electrospray ionization high-resolution tandem mass spectrometry (nanoLC-ESI-HRMS²). The results were expressed as number of O^6 MeG per 10^7 nucleotides (nt). The results were then converted to O^6 MeG per cell. The calculation rests on the measured DNA content of 5.11 pg DNA per cell in the exponentially growing A172 population, and 8.22 pg DNA per cell in the exponentially growing LN229 population. It further rests on the relationship of 1 pg DNA corresponding to 10^9 bp (2×10^9 nt), which gives rise to the following equation: $O^6\text{MeG}/10^7\text{nt} \times \text{pg DNA/cell} \times 2 \times 10^9\text{nt/pg}$.

Quantification of apoptosis and necrosis

The fraction of apoptotic and necrotic cells was determined using annexin V and propidium iodide (A/PI) staining of cells and measured by flow cytometry. For analysis, trypsinized cells including the supernatant were collected, transferred into 15 mL falcon tubes, washed with PBS, and stored on ice. For labeling, cells were incubated for 15 minutes at RT in 50 μL $1 \times$ annexin binding buffer containing 2.5 μL annexin V/FITC (MiltenyiBiotec GmbH). For PI staining, 10 μL PI from a 1 mg/mL stock solution (Sigma-Aldrich) and annexin binding buffer were added to each sample. Cells were incubated for additional 10 minutes on ice. Cells were kept in the dark until measurement. Data acquisition was performed using the FACS Canto II flow cytometer (Becton Dickinson GmbH) and the data were analyzed using the

Flowing Software 2 program (PerttuTerho, Turku Center for Biotechnology, University of Turku, Finland). Apoptotic cells were defined as Annexin V⁺/PI⁻ cells, whereas late apoptotic/necrotic cells were defined as Annexin V⁺/PI⁺ cells. For the sake of simplicity, this fraction is simply called “necrosis.” A representative plot showing the Annexin V⁺/PI⁻ and Annexin V⁻/PI⁺ fractions is shown in Supplementary Fig. S1.

Quantification of cellular senescence

Induced senescence was determined by the amount of cellular SA- β -galactosidase. To inhibit endogenous β -galactosidase activity, cells were pre-incubated with 300 μ mol/L chloroquine for 30 minutes in the incubator after which C₁₂FDG was added to each sample at a final concentration of 33 μ mol/L. Following a 90 minutes incubation period, cells were washed once with cold PBS and collected by trypsinization. Cell pellets were washed again with cold PBS, resuspended in cold PBS, and stored on ice. After the addition of chloroquine, cells were kept in the dark up to harvest. Data acquisition was performed using the FACS Canto II flow cytometer (Becton Dickinson GmbH) and the data were analyzed using the Flowing Software 2 program (PerttuTerho, Turku Center for Biotechnology, University of Turku). Untreated cells served as control. The cell population showing SA- β -GAL mediated staining higher than the control was defined as senescent.

Quantification of γ H2AX and 53BP1 foci

The γ H2AX and 53BP1 foci assays were conducted essentially as described (34). Evaluation of γ H2AX and 53BP1 stained nuclei of cells grown on coverslips occurred by LSM from a single focus plane. At least 100 cells were assessed per experiment and all experiments were performed three times independently. Antibodies used were γ H2AX

(1:500, rabbit; Cell Signaling Technology, mAb #9718S) combined with Cy3 goat-anti-rabbit (1:500; Abcam, ab97075) and 53BP1 (1:500, mouse, Sigma-Aldrich, MAB 3802) combined with Alexa Fluor 488 goat-anti-mouse (1:500, Thermo Fisher Scientific Invitrogen, A11017). The foci were counted with the software ImageJ (Wayne Rasband, NIH).

Statistical analysis and mathematic assessments

Data are presented as mean of at least three independent experiments \pm SEM and compared by unpaired *t* test with Welch's correction. The calculation of O⁶MeG levels per cell was described above.

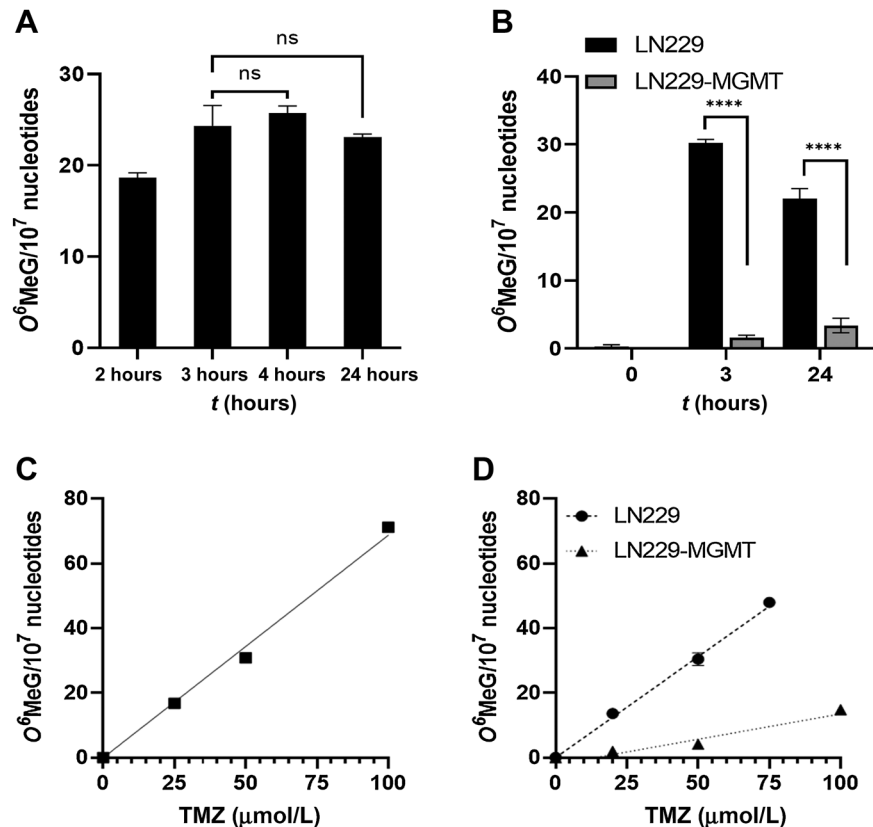
Results

Amount of O⁶MeG induced by TMZ

To relate phenotypic effects of TMZ exposure with primary adduct formation, first we determined the amount of O⁶MeG formed in glioblastoma cells following treatment with TMZ. The drug has a half-life of 1.9 hours in serum (35) and, therefore, even chronic exposure can be considered as pulse-treatment. To establish the optimal time of treatment for determining the alkylation level, we exposed cells to TMZ for different durations. As shown in Fig. 1A, O⁶MeG was induced in LN229 cells, which are MGMT repair incompetent, with a maximum level 3 to 4 hours after addition of 50 μ mol/L TMZ to the medium and did not further increase due to the short half-life of the drug in the medium. In a separate series of experiments, we compared LN229 with LN229 stably transfected with human MGMT (LN229-MGMT) and observed that the amount of O⁶MeG was significantly lower in MGMT-expressing cells even 3 hours after the onset of treatment (Fig. 1B), which was expected as MGMT performs a fast repair reaction (36).

Figure 1.

Amount of O⁶MeG induced in glioblastoma cells (LN229) upon treatment with TMZ. **A**, Adducts induced after 2, 3, 4, and 24 hours exposure of LN229 cells with 50 μ mol/L TMZ. There is no significant difference between the levels. Amount of adducts induced in LN229 and LN229-MGMT cells exposed for 3 and 24 hours to 50 μ mol/L TMZ. Data are the mean of three independent determinations \pm SEM ($P < 0.0001$). O⁶MeG in glioblastoma cells exposed to TMZ for 3 hours in A172 cells (**C**) and in LN229 and LN229-MGMT cells (**D**). Data are the mean of three independent determinations \pm SEM. A172: $y = 0.6873 \times x$; LN229: $y = 0.6239 \times x$; LN229-MGMT: $y = 0.1569 \times x - 2.151$. ns, not significant.



After having established the optimal treatment time for adduct quantification to be 3 hours, we determined the dose-response relationship for the induction of O^6 MeG. The amount of O^6 MeG in the DNA of A172 cells increased as a linear function of TMZ dose (Fig. 1C). Similar data were obtained for LN229 (Fig. 1D). Thus, a dose of 50 $\mu\text{mol/L}$ TMZ induced 34 and 31 O^6 MeG/ 10^7 nucleotides in A172 and LN229 cells, respectively (for a direct comparison of A172 and LN229 see Supplementary Fig. S2). A172 and LN229 do not express MGMT due to MGMT promoter hypermethylation and are unable to repair O^6 MeG (37). Therefore, we used MGMT transfected cells and found that O^6 MeG could not be detected if cells were treated with doses below 50 $\mu\text{mol/L}$ (Fig. 1D), indicating efficient and complete repair of the damage in this low-dose range. At high dose levels, however, a small increase in O^6 MeG was recorded (Fig. 1D), indicating increasing saturation of repair activity.

DSBs induced by TMZ

A highly sensitive and generally accepted method of detecting DSBs is based on the phosphorylation of histone 2AX (H2AX) around the DNA break, which is catalyzed by damage-activated ATR and ATM proteins, resulting in immuno-detectable nuclear foci (γ H2AX). At the same time, 53BP1, an accessory protein supporting the repair of DSBs, becomes phosphorylated and recruited to the DSB sites. Thus, γ H2AX foci and colocalized 53BP1 foci are considered to be reliable marker of

DSBs. Therefore, we quantified γ H2AX and 53BP1 foci (for representative images see Fig. 2A) in cells exposed to TMZ. The dose-response curves shown in Fig. 2B–D demonstrate a linear increase of foci without a threshold. Thus, already a low dose of 5 $\mu\text{mol/L}$ TMZ gave rise to a significant increase in the DSBs, as measured 72 hours after TMZ treatment in A172 cells.

Induction of the DNA damage response: p53 and p21

It is well established that DSBs trigger the DNA damage response (DDR), which targets downstream p53, phosphorylating p53 at serine 15. This phosphorylation leads to nuclear translocation, trimerization, and activation of p53 as transcription factor. One of the p53 target genes is p21, which is a key player in cell-cycle regulation. As shown in Fig. 3, p53ser15 and concomitantly p21 are upregulated dose-dependently until reaching a saturation level, which is achieved with a dose of about 10 to 15 $\mu\text{mol/L}$ TMZ (Fig. 3A for a representative Western blot analysis, Fig. 3B for total p53 and Fig. 3C and D for the dose-response curves of p53ser15 and p21).

Mathematical analysis of the linear dose range (0–15 $\mu\text{mol/L}$) did not reveal a no-effect threshold dose (Fig. 3E and F). It should be noted that total p53 protein was not enhanced (Fig. 3B), which is due to the fact that p53 is mutated in A172 cells, leading to its stabilization without having impact on its trans-activating activity.

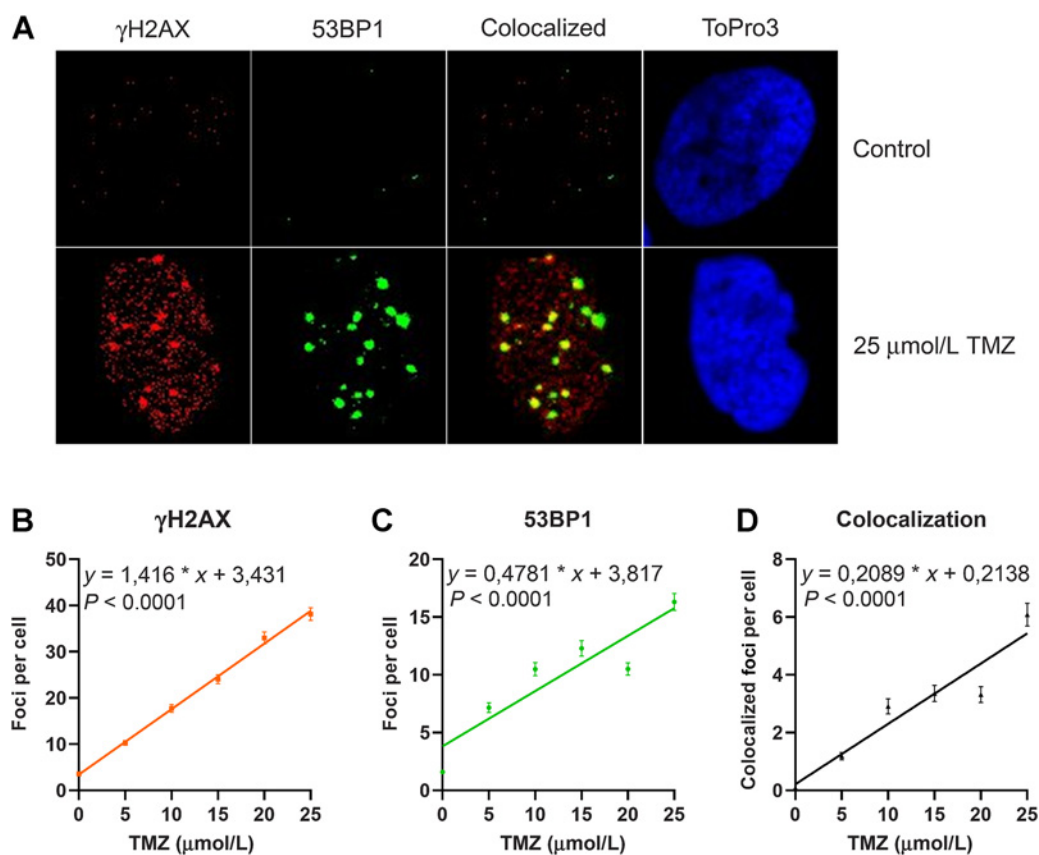
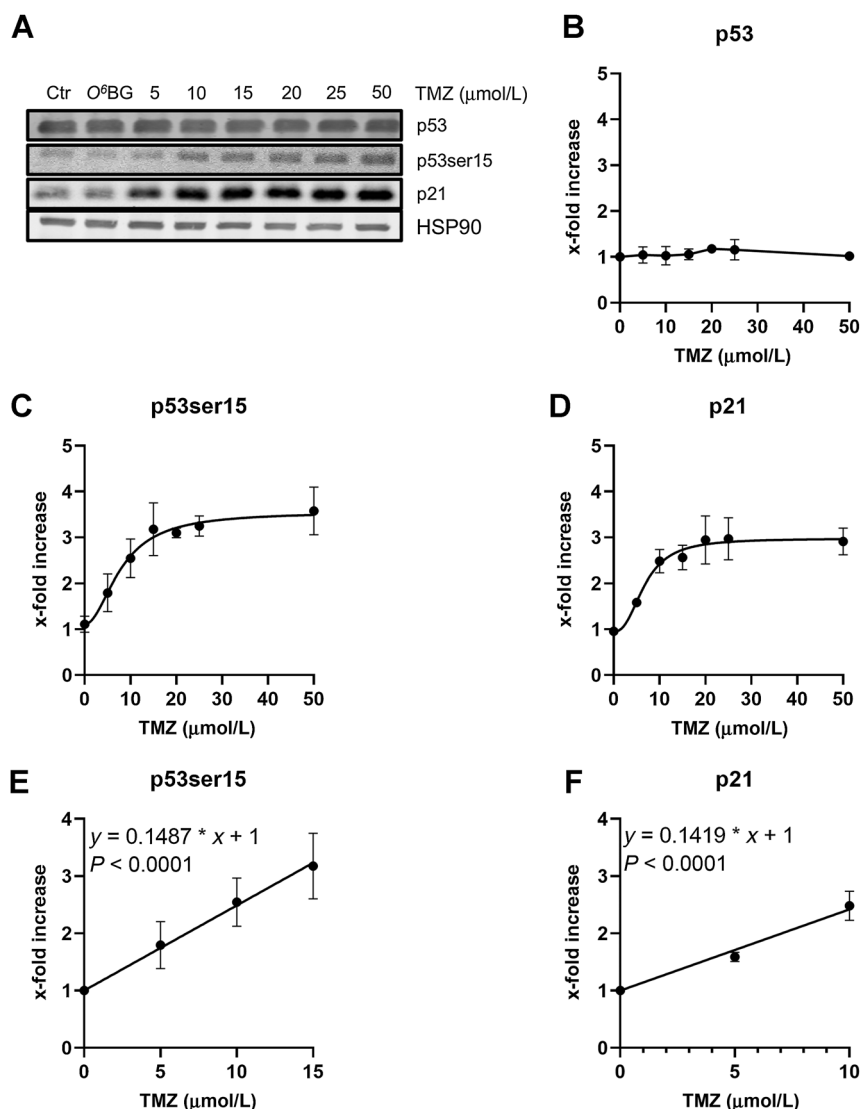


Figure 2.

Amount of γ H2AX and 53BP1 foci induced in A172 glioblastoma cells upon treatment with increasing doses of TMZ. Cells were fixed and immunostained 72 hours after the addition of TMZ to the medium. **A**, Images of representative examples. Dose response for γ H2AX (**B**), 53BP1 (**C**), and colocalized foci (**D**). Data are the mean of four independent determinations \pm SEM. The following equations describe the curves for γ H2AX $y = 1.416 \times x + 3.431$, for 53BP1 $y = 0.4781 \times x + 3.817$, for colocalized foci $y = 0.2089 \times x + 0.2138$.

Figure 3.

Amount of p53, p53ser15, and p21 in A172 cells treated with various doses of temozolomide. **A**, Exponentially growing cells were harvested 120 hours after treatment with TMZ. HSP90 was used as loading control. A representative Western blot analysis is shown. Quantification of p53 (**B**), p53ser15 (**C**), and p21 (**D**) in A172 cells treated with TMZ. Data are the mean of three independent experiments \pm SEM. Dose response for p53ser15 (**E**) and p21 (**F**) in A172 cells at the low TMZ dose range (up to 15 $\mu\text{mol/L}$). The curves do not indicate a threshold dose.



Induction of apoptosis and necrosis by TMZ

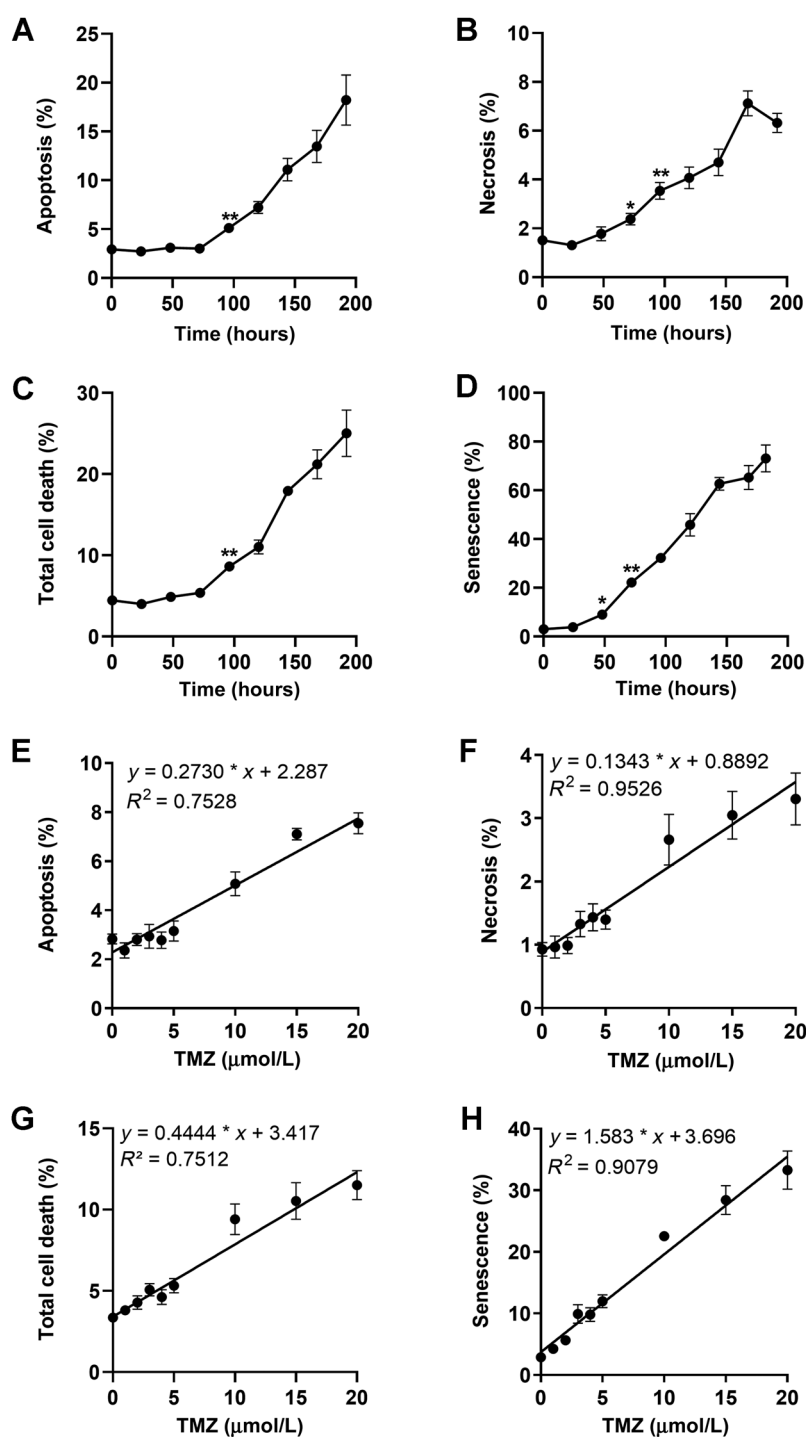
As previously shown, the induction of DSBs triggered by O⁶MeG precedes the activation of cell death pathways, which is a late response following DNA damage (23). The time course of apoptosis, necrosis, total cell death, and induced cellular senescence of A172 cells is shown in **Fig. 4**, demonstrating that cell death by apoptosis (**Fig. 4A**) and necrosis (**Fig. 4B**) starts at 96 hours significantly above the control level and increases thereafter continuously. The onset of cellular senescence was observed earlier (**Fig. 4D**; significant increase 48 hours after treatment $P < 0.05$). On the basis of these data, we decided to measure for the influence of TMZ dose on these endpoints 120 hours after addition of TMZ to the medium.

We measured the rate of apoptosis, necrosis, and total cell death upon treatment with TMZ using a dose range of up to 50 $\mu\text{mol/L}$. We used defined seeding conditions to ensure exponential growth over the whole post-exposure period. As shown in the Supplementary data (Supplementary Fig. S3), apoptosis increased up to a level of max. 8% and then reached saturation at a dose of 20 $\mu\text{mol/L}$. In contrast, necrosis increased over the whole dose range linearly

up to a level of 7% at 50 $\mu\text{mol/L}$. Because necrosis was a minor trait, the total cell death level reached saturation at 20 $\mu\text{mol/L}$. Induced senescence increased up to 30% to 40% and reached a saturation level at 20 $\mu\text{mol/L}$ (Supplementary Fig. S3). Having established the linear dose range, we conducted further experiments using the dose range of 0 to 20 $\mu\text{mol/L}$ TMZ. As shown in **Fig. 4E–F**, apoptosis, necrosis, and total cell death increased as a linear function of dose. An analysis of the data on the basis of the hockey stick model (38) revealed a possible threshold at 2.5 $\mu\text{mol/L}$ for the endpoint apoptosis, whereas for necrosis a significant threshold was not detected (see Supplementary Fig. S4).

Cellular senescence induced by TMZ

Similar experiments were performed with the endpoint cellular senescence, which was quantified by C₁₂FDG-flow cytometry. The level of senescence increased again as a linear function of dose. For senescence no threshold was observed (**Fig. 4H**), which was confirmed by hockey stick modeling of the data (Supplementary Fig. S5).

**Figure 4.**

Time-course of apoptosis (**A**), necrosis (**B**), total cell death (**C**), and senescence (**D**) after treatment with 50 $\mu\text{mol/L}$ TMZ of A172. Data are the mean of at least three independent experiments \pm SEM (*, $P < 0.05$; **, $P < 0.01$). Dose response of apoptosis (**E**), necrosis (**F**), and total cell death (**G**) in A172 cells treated with TMZ and measured 120 hours after the start of treatment. Data are the mean of five independent experiments measured in duplicate \pm SEM. **H**, Cellular senescence ($\text{C}_{12}\text{FDG}^+$) induced by TMZ in A172 cells. Data are the mean of four independent experiments \pm SEM.

Correlation between $O^6\text{MeG}$ and DSBs, cell death, and senescence

Next, we wished to know how many $O^6\text{MeG}$ lesions per cell give rise to a DSB and cytotoxic effects. To this end, we recalculated the amount of $O^6\text{MeG}$ per unit DNA into $O^6\text{MeG}$ adducts per cell. The DNA content per cell was determined on the basis of the amount of DNA extracted from a given number of cells in an exponentially growing population; 5.11 and 8.22 pg DNA per cell for A172 and LN229,

respectively. The dependence of γH2AX , 53BP1, and colocalized foci with the level of induced $O^6\text{MeG}$ adducts per cell are shown in **Fig. 5A–C**, respectively, for a dose range up to 25 $\mu\text{mol/L}$ TMZ. Assuming a 1:1 relation between γH2AX foci and DSBs, we estimated for A172 cells that 490 $O^6\text{MeG}$ adducts per cell are required to induce one DSB (calculated from the slope of regression). Assuming that one $\gamma\text{H2AX}/53\text{BP1}$ colocalized focus corresponds to one DSB, about 3,350 adducts are required for inducing one DSB.

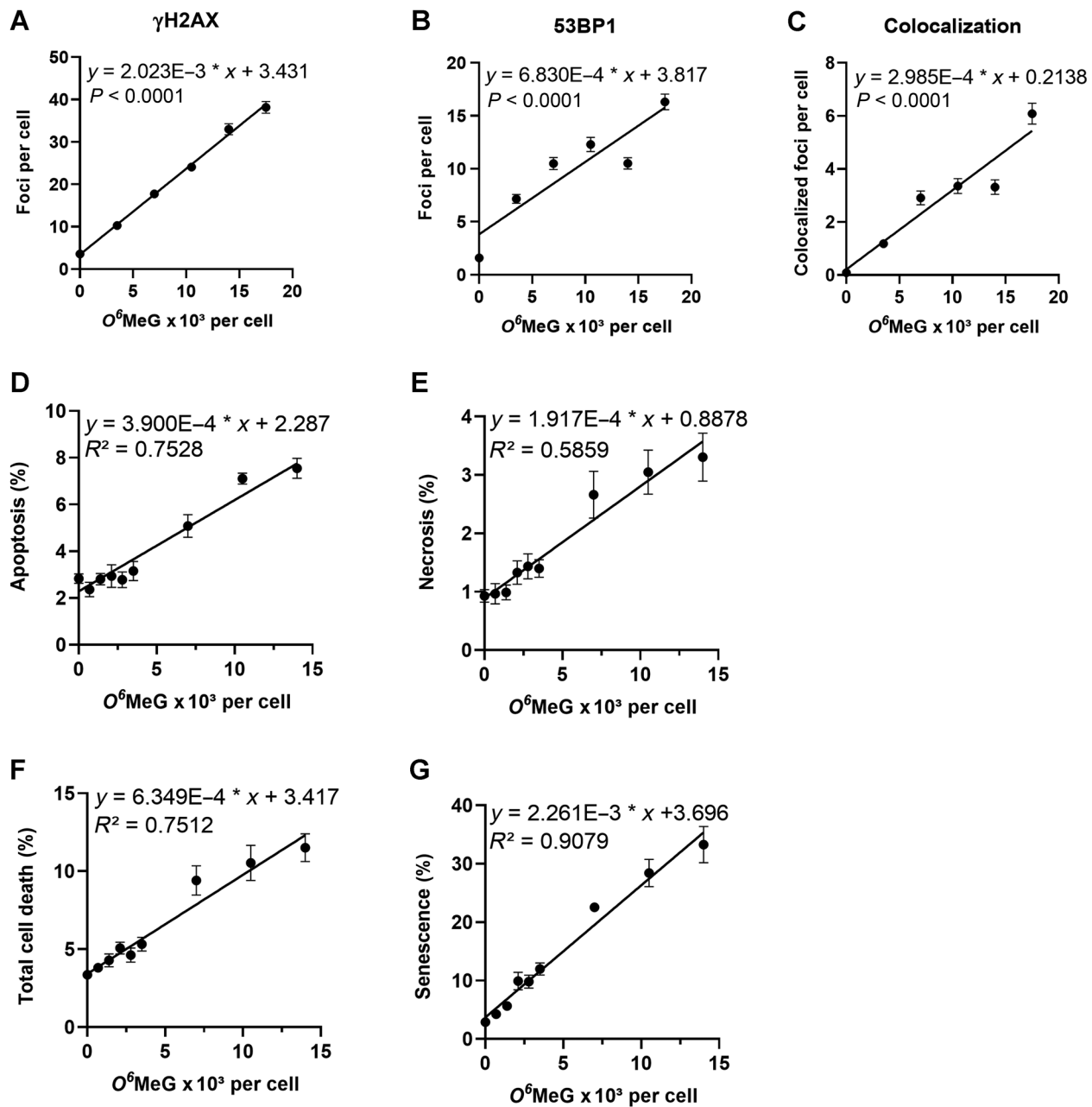


Figure 5.

Cellular responses as a function of $O^6\text{MeG}$ induced by TMZ in A172 glioblastoma cells. γH2AX (A), 53BP1 (B), colocalized foci (C), apoptosis (D), necrosis (E), total cell death (F), senescence (G) as a function of the $O^6\text{MeG}$ content per cell. Data are from Figs. 1 to 4.

The dose–response relationships for apoptosis, necrosis, total cell death, and senescence with $O^6\text{MeG}$ adducts per cell are presented in Fig. 5D to G for a dose range up to 20 $\mu\text{mol/L}$. From this we calculated that an increase by 1% in the population of apoptotic cells requires 2,560 $O^6\text{MeG}$ adducts per cell, of necrosis 5,220 $O^6\text{MeG}$, and total cell death 1,580 $O^6\text{MeG}$ per cell. A 1% increase of cells undergoing senescence requires only 440 $O^6\text{MeG}$ adducts per cell. It is important to note that senescence is the major endpoint triggered by $O^6\text{MeG}$ lesions (7.5% apoptosis and 3.5% necrosis compared with 35% senescence 120 hours after TMZ treatment)

and, therefore, a lower amount of $O^6\text{MeG}$ adducts is required to trigger this response.

$O^6\text{MeG}$ and responses triggered in LN229 cells

The same modeling of the relationship of various cellular responses with drug-induced adduct levels was performed for the widely used and well-characterized glioblastoma cell line LN229 (MGMT lacking, p53 functionally wt). The $O^6\text{MeG}$ adduct levels (calculated from the dose–response curve in Fig. 1) were related to DSBs, apoptosis, and senescence values from our previous

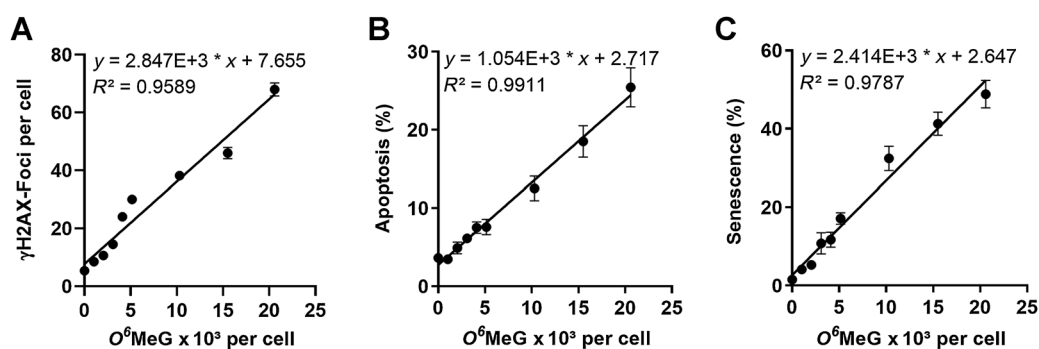


Figure 6.

Responses induced in LN229 cells by TMZ in dependence on the amount of $O^6\text{MeG}$ per cell: γH2AX (A), apoptosis (B), and senescent cells (C) in the population following treatment with increasing concentrations of TMZ. Data are from Fig. 1, ref. 34, and Supplementary Materials and Methods.

report (34) and supplementary data (Supplementary Fig. S6). The data revealed that γH2AX foci (Fig. 6A), apoptosis (Fig. 6B), and senescence (Fig. 6C) increased linearly with the $O^6\text{MeG}$ adduct level per cell, and no thresholds were apparent. In this case, an increase of apoptosis by 1% in the population was calculated to require 950 $O^6\text{MeG}$ adducts per cell, and senescence 410 $O^6\text{MeG}$ adducts per cell. Assuming a 1:1 correlation between γH2AX foci and DSBs, we calculated that 350 $O^6\text{MeG}$ adducts are required for the induction of one DSB in LN229 cells. LN229 cells expressing MGMT were completely refractory to the induction of γH2AX foci, apoptosis, and senescence (Supplementary Fig. S6).

Discussion

TMZ, front-line drug in the treatment of high-grade malignant glioma, is effective if the tumor lacks MGMT or expresses the repair protein at a low level (<30 fmol/mg protein) (39). These tumors are defined as “methylated” because MGMT promoter CpG methylation correlates with silencing of the gene (40) and, as a consequence, lack of or low MGMT protein expression and enzyme activity (17). Although the curative effect is significant, the response is not dramatic and the prognosis of GBM is still bleak with a median survival of only 14.6 months (12.6 and 23.4 months in the MGMT-unmethylated and MGMT-methylated subgroups, respectively; ref. 41). Although recent phase III clinical trials revealed that the median overall survival for adult patients with newly diagnosed GBM can reach up to 20 months, indicating a trending increase in survival, the prognosis is still bad with 5-year overall survival rates of less than 10% (42). Given the mechanism of action of TMZ and the low curative response, some questions arise which are in the literature controversially discussed (27, 30) and thus need to be addressed experimentally. (i) Do GBM cells really die (by apoptosis or other forms of cell death) following TMZ treatment or does the drug just exert a cytostatic effect? (ii) Are the doses used for patient’s treatment high enough to kill cancer cells in their body? This question implies that low doses are ineffective and that threshold doses do exist below which cytotoxicity does not occur. (iii) How many $O^6\text{MeG}$ adducts are required for eliciting a specific effect such as apoptosis, necrosis, and senescence? Here, we present data on the amount of $O^6\text{MeG}$ induced by TMZ in established GBM cell lines and set it in relation to the level of DSBs, apoptosis, necrosis, overall cell death, and cellular senescence.

Endpoints triggered by $O^6\text{MeG}$

MGMT-lacking GBM cells respond to treatment with TMZ in the dose range up to 50 $\mu\text{mol/L}$ with the induction of apoptosis, autophagy, and senescence. These effects were nearly completely vanished in isogenic MGMT expressing cells (Supplementary Fig. S6), supporting that $O^6\text{MeG}$ induced by TMZ is responsible for these endpoints (8). Because autophagy is a survival pathway and cellular senescence a cytostatic effect, it is pertinent to conclude that $O^6\text{MeG}$ triggers both survival and death pathways. The apoptosis pathways triggered by $O^6\text{MeG}$ are well described (25, 27); they involve activation of both the death receptor FAS/CD95/APO1 and the intrinsic mitochondrial pathway, dependent on the cellular background (43). Recently we showed, using LN229 cells, that apoptosis is a linear function of dose (34), which was substantiated in the present work with A172 cells. Using hockey-stick modeling (38), we show that there is no threshold for TMZ/ $O^6\text{MeG}$ -induced apoptosis in LN229 cells, and a marginal threshold in A172 cells at a dose level of 2.5 $\mu\text{mol/L}$. In MGMT expressing cells the threshold is clearly higher, dependent on the MGMT expression level. Previous work with isogenic cell strains expressing different MGMT levels showed that the protection caused by the repair protein is a linear function of MGMT molecules per cell (4). Comparing the different endpoints triggered by $O^6\text{MeG}$ quantitatively, it is interesting to note that the yield of cell death by apoptosis (and necrosis, which represents a minor fraction) is significantly lower than senescence. Thus, we measured 120 hours after TMZ treatment in LN229 cells 25.4% apoptosis and 48.8% senescence, and in A172 cells 7.5% apoptosis and 33.3% senescence. Similar to apoptosis, senescence increased linearly with dose, without a no-effect threshold. Overall, $O^6\text{MeG}$ elicits both a cytotoxic and cytostatic effect by activating, in the same dose range, the apoptosis and the senescence pathway; the latter is the predominant trait. This occurs already at low dose levels (<50 $\mu\text{mol/L}$), which can be achieved *in vivo* in a therapeutic setting (44).

Is TMZ effective in killing cancer cells *in vivo*?

Treatment of patients with TMZ occurs daily by different schedules (2, 29, 45, 46). The serum half-life of TMZ is about 2 hours and the serum concentration of TMZ has been determined to be in the range of 20 to 70 $\mu\text{mol/L}$ (1, 47–51). Thus, in a therapeutic setting with a single oral dose of 150 mg/m^2 , the peak plasma concentration was, on average, 28.4 $\mu\text{mol/L}$ (5.5 $\mu\text{g/mL}$) and the brain interstitium concentration was 1.5 $\mu\text{mol/L}$ (0.3 $\mu\text{g/mL}$; ref. 52). In another study, following oral 200 mg/m^2 TMZ, the plasma peak level was 72 $\mu\text{mol/L}$, and

the concentration in the cerebrospinal fluid was 9.9 $\mu\text{mol/L}$ (53). Overall, the TMZ concentration at the target organ seems to be rather low (1–10 $\mu\text{mol/L}$), which may lead to the conclusion that the TMZ alkylation level is not high enough to exert a cytotoxic effect on GBM cells. Given the fact that p53 plays a supporting role in apoptosis and senescence triggered by $O^6\text{MeG}$ (31, 37), the supposition is nourished by the assumption that DNA damage activated p53 pathways involving p53ser15 and HIPK2/p53ser46 play a protective role at a low, and a proapoptotic role at a high genotoxin level, respectively (54). This model implicates that thresholds exist that regulate the balance between life and death (44). Therefore, we expected that cell death is not induced at low DNA damage levels. The view that TMZ is rather ineffective in glioma treatment is further fueled by the supposition that TMZ exerts only cytostatic, but not cytotoxic activity (30).

Here, using the well-characterized glioblastoma cell lines A172 and LN229, we show that the amount of $O^6\text{MeG}$ in the DNA and the number of DSBs increase linearly with dose of TMZ, and the same was observed for apoptosis and senescence. We did not observe a threshold for DSBs (as measured by γH2AX and 53BP1 foci formation), apoptosis, necrosis, and senescence (see also our previous report; ref. 34). This finding has implications regarding underlying mechanisms. It indicates that upon DDR activation by $O^6\text{MeG}$ -triggered secondary lesions (i.e., MMR-mediated gaps and DSBs resulting from them during replication) cells make a decision between survival and death in a stochastic manner and, at least in this cell system, there does not appear to be a threshold dose below which cell death pathways are not activated. Interestingly, at all dose levels we observed the induction of apoptosis and senescence, indicating that in the cell population cytotoxic and cytostatic effects are brought about at the same time by the same critical lesion $O^6\text{MeG}$, although to a different extent. If we translate these findings to the tumor *in vivo*, we can posit that even at a low concentration TMZ elicits a cytotoxic (apoptosis and at very low degree necrosis) and a cytostatic (senescence) effect. It should also be considered the possibility that repeated low-dose treatment leads to an accumulation of $O^6\text{MeG}$ in MGMT-deficient tumor cells and an amelioration of the cytotoxic effects. This supposition is currently under study. Overall, the findings strongly support the view that repetitive treatments with low doses of TMZ (according to the metronomic schedule) are effective and represent a reasonable treatment strategy.

How many $O^6\text{MeG}$ adducts are required for inducing DSBs, p53ser15, apoptosis, necrosis, and senescence?

Here, we have quantified for the first time $O^6\text{MeG}$ adducts induced by TMZ in glioblastoma cells and set it in relation to the amount of DSBs, p53ser15, apoptosis, necrosis, and cellular senescence. From the corresponding dose–response curves, we calculated the amount of $O^6\text{MeG}$ adducts that are required for eliciting a specific effect. The results are compiled in **Table 1**. The data show that 48 and 21 $O^6\text{MeG}/10^7$ nt give rise to 1 DSB (measured by a γH2AX focus) in A172 and LN229 cells, respectively. This corresponds to 490 and 350 $O^6\text{MeG}$ per cell that result in a DSB in A172 and LN229, respectively. The formation of one 53BP1 focus needs 1,460 $O^6\text{MeG}$, and colocalized foci were observed at a level of 3,350 $O^6\text{MeG}$ in A172 cells. A twofold increase of phosphorylated p53ser15 needed 4,700 $O^6\text{MeG}$, a twofold increase in p21 4,830 $O^6\text{MeG}$, and an increase in apoptosis by one percent required an adduct level of 2,560 and 950 $O^6\text{MeG}$ in A172 and LN229, respectively. Necrosis was measured only in A172, and an increase by 1% was seen at 5,220 $O^6\text{MeG}$. Overall, for inducing 1% cell death (apoptosis and necrosis) about 1,580 $O^6\text{MeG}$ adducts are needed. Senescence is triggered already by lower amounts of $O^6\text{MeG}$, with 440 and 410 $O^6\text{MeG}$ adducts needed for increasing the senescence level by 1% in A172 and LN229 cells, respectively.

In **Table 1**, we also show the effect level brought about by a dose of 20 $\mu\text{mol/L}$ TMZ, which induces 14,000 and 20,600 adducts per cell in A172 and LN229, respectively. This dose induced 32 DSBs (γH2AX foci) per A172 cell, a 3-fold increase of p53ser15 (which was saturated already with a dose of 15 $\mu\text{mol/L}$ TMZ), a 3-fold increase in p21 (saturated at a dose level of 10 $\mu\text{mol/L}$ TMZ). Under these conditions, 12.3% of cells were dead and 35.4% of cells showed the senescence phenotype as measured 120 hours after the onset of treatment. Overall, this low-dose caused significant genotoxic and cytotoxic effects. It should be noted that long-term cultivation of TMZ-treated cells resulted in cell loss in the subsequent passages, which is explained by $O^6\text{MeG}$ triggered cell death in >2 posttreatment cell cycles, as demonstrated previously (10).

$O^6\text{MeG}$ is a most interesting DNA damage as it is not only cytotoxic, but also able to trigger genotoxic end points such as sister chromatid-exchanges (SCE), point mutations, chromosomal aberrations, and DNA single- and DSBs. In previous work, it was shown that O^6 -methylating agents require two cell cycles for SCEs to be formed, indicating secondary lesions to be involved (55). This was

Table 1. DSBs represented by γH2AX and 53BP1 foci, cell death, and cellular senescence induced in A172 and LN229 cells upon treatment with TMZ dependent of $O^6\text{MeG}$ adducts per cell.

Effect	A172		LN229	
	$O^6\text{MeG}$ per cell	Effects triggered by 14,000 $O^6\text{MeG}$ per cell (20 $\mu\text{mol/L}$ TMZ)	$O^6\text{MeG}$ per cell	Effects triggered by 20,600 $O^6\text{MeG}$ per cell (20 $\mu\text{mol/L}$ TMZ)
γH2AX	490 per focus	32 foci	350 per focus	66 foci
53BP1	1,460 per focus	13 foci	nd	nd
Colocalization	3,350 per focus	4 foci	nd	nd
p53ser15	4,700 per 2-fold	3-fold ^a	nd	nd
p21	4,830 per 2-fold	3-fold ^b	nd	nd
Apoptosis	2,560 per 1% increase	7.7%	950 per 1% increase	24.4%
Necrosis	5,220 per 1% increase	3.6%	nd	nd
Total cell death	1,580 per 1% increase	12.3%	nd	nd
Senescence	440 per 1% increase	35.4%	410 per 1% increase	52.4%

Note: Data are from **Figs. 5** and **6**.

Abbreviation: nd, not determined.

^aSaturated at 10,500 $O^6\text{MeG}$ lesions.

^bSaturated at 7,000 $O^6\text{MeG}$ lesions.

confirmed using MGMT-isogenic cell lines, demonstrating that critical events are happening in the posttreatment cell cycle (56). The conversion probability for O^6 MeG into SCEs was determined in two independent studies: in MGMT lacking CHO-9 cells it was shown that 30 O^6 MeG per cell give rise to 1 SCE (57) whereas for a glioblastoma cell line the relationship was 43 O^6 MeG/SCE (58). This is a very high conversion rate compared with other DNA lesions, for example, UV-induced pyrimidine dimers with 600 adducts/SCE (59). Regarding cytotoxicity, from the slope of survival curves (colony formation) it was estimated that 6,650 O^6 MeG induce one lethal hit (58). It is important to note that colony formation, which is frequently used as a highly sensitive indicator of cytotoxicity, is biased by the fact that nontoxic events such as cell-cycle inhibition and induced senescence reduce the size and number of colonies and therefore simulate cytotoxicity. For this reason, survival curves on the basis of colony formation can hardly be compared with dose-response curves based on apoptosis and necrosis, which are clear cell death indicators. Although the amount of O^6 MeG induced in A172 and LN229 cells was rather similar, the amount of DSBs and the levels of apoptosis and induced senescence were not identical, which is expected in view of the complex pathways involved, including the conversion of O^6 MeG into critical secondary lesions, triggering the DDR and activation of survival and death pathways.

Conclusions

O^6 MeG is a highly recombinogenic, mutagenic, genotoxic, autophagy, senescence, and apoptosis-inducing lesion (4, 5, 8, 25). It triggers with high efficiency SCE formation, which are cytogenetic events resulting from a damage tolerance process (60), followed by DSBs, senescence, and apoptosis. The linear dose-effect relationship for O^6 MeG and DSBs strongly indicates that in the therapeutic dose range, glioblastoma cells *in vivo* are damaged, causing responses that include cell death and cellular senescence, which appears to be the major trait. Because the O^6 MeG/MMR/DSB-triggered downstream survival and death pathways of senescence and apoptosis are activated at the same time in the cell population, complete elimination of cancer

cells cannot be expected by this therapeutic strategy. The possibility of senescent cells being reactivated to go back into cycle and start to proliferate must also be considered. Furthermore, TMZ-induced senescent glioblastoma cells secrete proinflammatory cytokines (26), which may drive tumorigenesis. Therefore, the elimination of senescent cells by senolytic drugs should be a further goal to improve therapeutic efficacy, as opposed to purely increasing the dose of TMZ in target tumor tissue. Finally, it is reasonable to postulate that quantitative adduct formation could serve as a potential biomarker of response and/or a determinant of adequate TMZ intratumoral dose. Therefore, molecular dosimetry of O^6 MeG in relation to cellular effects is important for elucidating critical damage levels in cancer and normal tissues during and after therapy.

Authors' Disclosures

S.J. Sturla reports grants from Swiss National Science Foundation and Swiss Cancer Research Foundation during the conduct of the study. B. Kaina reports grants from Deutsche Forschungsgemeinschaft and Deutsche Krebshilfe during the conduct of the study. No disclosures were reported by the other authors.

Authors' Contributions

B. Stratenwerth: Data curation, formal analysis, validation. **S.M. Geisen:** Conceptualization, data curation, formal analysis, validation, investigation, methodology. **Y. He:** Data curation. **L. Beltzig:** Data curation, validation, methodology. **S.J. Sturla:** Formal analysis, supervision, funding acquisition, validation, methodology. **B. Kaina:** Conceptualization, resources, data curation, formal analysis, supervision, funding acquisition, validation, investigation, methodology, writing-original draft.

Acknowledgments

The study was supported by Deutsche Forschungsgemeinschaft (DFG KA 724/31-1), German Cancer Aid, Swiss National Science Foundation (185020, 186332), and the Swiss Cancer Research Foundation (KFS-4443-02-2018-R).

The costs of publication of this article were defrayed in part by the payment of page charges. This article must therefore be hereby marked *advertisement* in accordance with 18 U.S.C. Section 1734 solely to indicate this fact.

Received March 15, 2021; revised May 1, 2021; accepted June 25, 2021; published first July 12, 2021.

References

- Newlands E, Stevens M, Wedge S, Wheelhouse R, Brock C. Temozolomide: a review of its discovery, chemical properties, pre-clinical development and clinical trials. *Cancer Treat Rev* 1997;23:35-61.
- Stupp R, Mason WP, van den Bent MJ, Weller M, Fisher B, Taphoorn MJ, et al. Radiotherapy plus concomitant and adjuvant temozolomide for glioblastoma. *N Engl J Med* 2005;352:987-96.
- Villano JL, Seery TE, Bressler LR. Temozolomide in malignant gliomas: current use and future targets. *Cancer Chemother Pharmacol* 2009;64:647-55.
- Kaina B, Fritz G, Mitra S, Coquerelle T. Transfection and expression of human O^6 -methylguanine-DNA methyltransferase (MGMT) cDNA in Chinese hamster cells: the role of MGMT in protection against the genotoxic effects of alkylating agents. *Carcinogenesis* 1991;12:1857-67.
- Margison GP, Santibanez Koref MF, Povey AC. Mechanisms of carcinogenicity/chemotherapy by O^6 -methylguanine. *Mutagenesis* 2002;17:483-7.
- Beranek DT. Distribution of methyl and ethyl adducts following alkylation with monofunctional alkylating agents. *Mutation Res* 1990;231:11-30.
- Kaina B, Christmann M, Naumann S, Roos WP. MGMT: key node in the battle against genotoxicity, carcinogenicity and apoptosis induced by alkylating agents. *DNA Repair* 2007;6:1079-99.
- Knizhnik AV, Roos WP, Nikolova T, Quiros S, Tomaszowski KH, Christmann M, et al. Survival and death strategies in glioma cells: autophagy, senescence and apoptosis triggered by a single type of temozolomide-induced DNA damage. *PLoS One* 2013;8:e55665.
- Pegg AE. Repair of O^6 -alkylguanine by alkyltransferases. *Mutation Res* 2000;462:83-100.
- Quiros S, Roos WP, Kaina B. Processing of O^6 -methylguanine into DNA double-strand breaks requires two rounds of replication whereas apoptosis is also induced in subsequent cell cycles. *Cell Cycle* 2010;9:168-78.
- Christmann M, Kaina B. Transcriptional regulation of human DNA repair genes following genotoxic stress: trigger mechanisms, inducible responses and genotoxic adaptation. *Nucleic Acids Res* 2013;41:8403-20.
- Christmann M, Kaina B. Epigenetic regulation of DNA repair genes and implications for tumor therapy. *Mutat Res* 2019;780:15-28.
- Margison GP, Povey AC, Kaina B, Santibanez Koref MF. Variability and regulation of O^6 -alkylguanine-DNA alkyltransferase. *Carcinogenesis* 2003;24:625-35.
- Goth R, Rajewsky MF. Persistence of O^6 -ethylguanine in rat-brain DNA: correlation with nervous system-specific carcinogenesis by ethylnitrosourea. *Proc Natl Acad Sci U S A* 1974;71:639-43.
- Silber JR, Mueller BA, Ewers TG, Berger MS. Comparison of O^6 -methylguanine-DNA methyltransferase activity in brain tumors and adjacent normal brain. *Cancer Res* 1993;53:3416-20.
- Preuss I, Haas S, Eichhorn U, Eberhagen I, Kaufmann M, Beck T, et al. Activity of the DNA repair protein O^6 -methylguanine-DNA methyltransferase in human tumor and corresponding normal tissue. *Cancer Detect Prev* 1996;20:130-6.

17. Christmann M, Nagel G, Horn S, Krahn U, Wiewrodt D, Sommer C, et al. MGMT activity, promoter methylation and immunohistochemistry of pretreatment and recurrent malignant gliomas: a comparative study on astrocytoma and glioblastoma. *Int J Cancer* 2010;127:2106–18.
18. Esteller M, Garcia-Foncillas J, Andion E, Goodman SN, Hidalgo OF, Vanaclocha V, et al. Inactivation of the DNA-repair gene MGMT and the clinical response of gliomas to alkylating agents. *N Engl J Med* 2000;343:1350–4.
19. Hegi ME, Diserens AC, Gorlia T, Hamou MF, de Tribolet N, Weller M, et al. MGMT gene silencing and benefit from temozolomide in glioblastoma. *N Engl J Med* 2005;352:997–1003.
20. Switzeny OJ, Christmann M, Renovanz M, Giese A, Sommer C, Kaina B. MGMT promoter methylation determined by HRM in comparison to MSP and pyrosequencing for predicting high-grade glioma response. *Clin Epigenetics* 2016;8:49.
21. Ensminger M, Iloff L, Ebel C, Nikolova T, Kaina B, Lbrich M. DNA breaks and chromosomal aberrations arise when replication meets base excision repair. *J Cell Biol* 2014;206:29–43.
22. Kaina B, Christmann M. DNA repair in personalized brain cancer therapy with temozolomide and nitrosoureas. *DNA Repair* 2019;78:128–41.
23. Ochs K, Kaina B. Apoptosis induced by DNA damage O6-methylguanine is Bcl-2 and caspase-9/3 regulated and Fas/caspase-8 independent. *Cancer Res* 2000;60:5815–24.
24. Eich M, Roos WP, Nikolova T, Kaina B. Contribution of ATM and ATR to the resistance of glioblastoma and malignant melanoma cells to the methylating anticancer drug temozolomide. *Mol Cancer Ther* 2013;12:2529–40.
25. He Y, Roos WP, Wu Q, Hofmann TG, Kaina B. The SIAH1-HIPK2-p53ser46 damage response pathway is involved in temozolomide-induced glioblastoma cell death. *Mol Cancer Res* 2019;17:1129–41.
26. Aasland D, Gotzinger L, Hauck L, Berte N, Meyer J, Effenberger M, et al. Temozolomide induces senescence and repression of DNA repair pathways in glioblastoma cells via activation of ATR-CHK1, p21, and NF-kappaB. *Cancer Res* 2019;79:99–113.
27. Kaina B. Temozolomide in glioblastoma therapy: role of apoptosis, senescence and autophagy. Comment on Strobel et al., temozolomide and other alkylating agents in glioblastoma therapy. *Biomedicines* 2019, 7, 69. *Biomedicines* 2019;7:90.
28. Anton K, Baehring JM, Mayer T. Glioblastoma multiforme: overview of current treatment and future perspectives. *Hematol Oncol Clin North Am* 2012;26:825–53.
29. Wick W, Winkler F. Regimen of procarbazine, lomustine, and vincristine versus temozolomide for gliomas. *Cancer* 2018;124:2674–6.
30. Strobel H, Baisch T, Fitzel R, Schilberg K, Siegelin MD, Karpel-Massler G, et al. Temozolomide and other alkylating agents in glioblastoma therapy. *Biomedicines* 2019;7:69.
31. Roos WP, Batista LFZ, Naumann S, Wick W, Weller M, Menck CFM, et al. Apoptosis in malignant glioma cells triggered by the temozolomide-induced DNA lesion O⁶-methylguanine. *Oncogene* 2007;26:186–97.
32. Kraus A, McKeague M, Seiwert N, Nagel G, Geisen SM, Ziegler N, et al. Immunological and mass spectrometry-based approaches to determine thresholds of the mutagenic DNA adduct O(6)-methylguanine in vivo. *Arch Toxicol* 2019;93:559–72.
33. Geisen SM, Aloisi CMN, Huber SM, Sandell ES, Escher NA, Sturla SJ. Direct alkylation of deoxyguanosine by azaserine leads to O(6)-carboxymethyldeoxyguanosine. *Chem Res Toxicol* 2021;34:1518–29.
34. He Y, Kaina B. Are there thresholds in glioblastoma cell death responses triggered by temozolomide? *Int J Mol Sci* 2019;20:1562.
35. Hammond LA, Eckardt JR, Baker SD, Eckhardt SG, Dugan M, Forral K, et al. Phase I and pharmacokinetic study of temozolomide on a daily-for-5-days schedule in patients with advanced solid malignancies. *J Clin Oncol* 1999;17:2604–13.
36. Pegg AE, Dolan ME, Moschel RC. Structure, function and inhibition of O6-alkylguanine-DNA-alkyltransferase. *Prog Nucleic Acid Res Mol Biol* 1995;51:167–223.
37. Hermisson M, Klumpp A, Wick W, Wischhusen J, Nagel G, Roos W, et al. O6-methylguanine DNA methyltransferase and p53 status predict temozolomide sensitivity in human malignant glioma cells. *J Neurochem* 2006;96:766–76.
38. Lutz WK, Lutz RW. Statistical model to estimate a threshold dose and its confidence limits for the analysis of sublinear dose-response relationships, exemplified for mutagenicity data. *Mutat Res* 2009;678:118–22.
39. Wiewrodt D, Nagel G, Dreimuller N, Hundsberger T, Pernecky A, Kaina B. MGMT in primary and recurrent human glioblastomas after radiation and chemotherapy and comparison with p53 status and clinical outcome. *Int J Cancer* 2008;122:1391–9.
40. Esteller M, Hamilton SR, Burger PC, Baylin SB, Herman JG. Inactivation of the DNA repair gene O6-methylguanine-DNA methyltransferase by promoter hypermethylation is a common event in primary human neoplasia. *Cancer Res* 1999;59:793–7.
41. Stupp R, Hegi ME, Mason WP, van den Bent MJ, Taphoorn MJ, Janzer RC, et al. Effects of radiotherapy with concomitant and adjuvant temozolomide versus radiotherapy alone on survival in glioblastoma in a randomised phase III study: 5-year analysis of the EORTC-NCIC trial. *Lancet Oncol* 2009;10:459–66.
42. Stepanenko AA, Chekhonin VP. Recent advances in oncolytic virotherapy and immunotherapy for glioblastoma: a glimmer of hope in the search for an effective therapy? *Cancers* 2018;10:492.
43. Roos WP, Kaina B. DNA damage-induced cell death: from specific DNA lesions to the DNA damage response and apoptosis. *Cancer Lett* 2013;332:237–48.
44. Oren M. Decision making by p53: life, death and cancer. *Cell Death Differ* 2003;10:431–42.
45. Wick W, Steinbach JP, Kuker WM, Dichgans J, Bamberg M, Weller M. One week on/one week off: a novel active regimen of temozolomide for recurrent glioblastoma. *Neurology* 2004;62:2113–5.
46. Strik HM, Marosi C, Kaina B, Neyns B. Temozolomide dosing regimens for glioma patients. *Curr Neurol Neurosci Rep* 2012;12:286–93.
47. Weller M, Steinbach JP, Wick W. Temozolomide: a milestone in the pharmacotherapy of brain tumors. *Future Oncol* 2005;1:747–54.
48. Batchelor T. Temozolomide for malignant brain tumours. *Lancet* 2000;355:1115–6.
49. Danson SJ, Middleton MR. Temozolomide: a novel oral alkylating agent. *Expert Rev Anticancer Ther* 2001;1:13–9.
50. Friedman HS, Kerby T, Calvert H. Temozolomide and treatment of malignant glioma. *Clin Cancer Res* 2000;6:2585–97.
51. Marzolini C, Decosterd LA, Shen F, Gander M, Leyvraz S, Bauer J, et al. Pharmacokinetics of temozolomide in association with fotemustine in malignant melanoma and malignant glioma patients: comparison of oral, intravenous, and hepatic intra-arterial administration. *Cancer Chemother Pharmacol* 1998;42:433–40.
52. Portnow J, Badie B, Chen M, Liu A, Blanchard S, Synold TW. The neuropharmacokinetics of temozolomide in patients with resectable brain tumors: potential implications for the current approach to chemoradiation. *Clin Cancer Res* 2009;15:7092–8.
53. Ostermann S, Csajka C, Buclin T, Leyvraz S, Lejeune F, Decosterd LA, et al. Plasma and cerebrospinal fluid population pharmacokinetics of temozolomide in malignant glioma patients. *Clin Cancer Res* 2004;10:3728–36.
54. Roos WP, Thomas AD, Kaina B. DNA damage and the balance between survival and death in cancer biology. *Nat Rev Cancer* 2016;16:20–33.
55. Kaina B, Aurich O. Dependency of the yield of sister-chromatid exchanges induced by alkylating agents on fixation time. Possible involvement of secondary lesions in sister-chromatid exchange induction. *Mutation Res* 1985;149:451–61.
56. Kaina B, Ziouta A, Ochs K, Coquerelle T. Chromosomal instability, reproductive cell death and apoptosis induced by O⁶-methylguanine in Mex-, Mex+ and methylation-tolerant mismatch repair compromised cells: facts and models. *Mutation Res* 1997;381:227–41.
57. Kaina B, Fritz G, Coquerelle T. Contribution of O⁶-alkylguanine and N-alkylpurines to the formation of sister chromatid exchanges, chromosomal aberrations, and gene mutations: new insights gained from studies of genetically engineered mammalian cell lines. *Environ Mol Mutagen* 1993;22:283–92.
58. Rasouli-Nia A, Sibghat U, Mirzayans R, Paterson MC, Day RS 3rd. On the quantitative relationship between O6-methylguanine residues in genomic DNA and production of sister-chromatid exchanges, mutations and lethal events in a Mer- human tumor cell line. *Mutat Res* 1994;314:99–113.
59. De Weerd-Kastelein EA, Keijzer W, Rainaldi G, Bootsma D. Induction of sister chromatid exchanges in xeroderma pigmentosum cells after exposure to ultraviolet light. *Mutat Res* 1977;45:253–61.
60. Kaina B. Mechanisms and consequences of methylating agent-induced SCEs and chromosomal aberrations: a long road traveled and still a far way to go. *Cytogenet Genome Res* 2004;104:77–86.